GW170817 constraints on the properties of a neutron star in the presence of WIMP dark matter

Abdul Quddus[1], Grigorios Panotopoulos[2], Bharat Kumar[3], Shakeb Ahmad[1], and S. K. Patra[4,5]
[1]*Department of Physics, Aligarh Muslim University, Aligarh - 202002, India*
[2]*Centro de Astrofísica e Gravitação, Departamento de Física, Instituto Superior Técnico-IST, Universidade de Lisboa-UL, Av. Rovisco Pais, 1049-001 Lisboa, Portugal*
[3]*Inter-University Centre for Astronomy and Astrophysics, Pune - 411007, India*
[4]*Institute of Physics, Sachivalaya Marg, Bhubaneswar - 751005, India and*
[5]*Homi Bhaba National Institute, Anushakti Nagar, Mumbai - 400085, India.*
(Dated: February 5, 2019)

The properties of neutron stars are studied in the presence of a dark matter core. We have considered a relatively light neutralino as a dark matter candidate with properties suggested by the results of the DAMA collaboration realized within the framework of the Next-to-Minimal Supersymmetric Standard Model. The neutralino interacts with baryonic matter of the neutron star through the Higgs boson. Dark matter variables are constrained from the results of DAMA experiments, which are used to construct the Lagrangian density for the neutralino-nucleon inside a neutron star. We have used the effective field theory motivated relativistic mean field model to study the equations-of-state in the presence of dark matter. The predicted equations-of-state are used in the TOV equations to obtain the mass-radius relations, moment of inertia, and effects of tidal field on a neutron star. The calculated properties are compared with the corresponding data of the GW170817 event.

PACS numbers: 95.35.+d, 26.60.Kp, 14.80.Da, 14.80.Nb

I. INTRODUCTION

One of the most chaotic and enthralling conundrum in physics is the problem of dark matter in the Universe. Several Cosmological and Astrophysical observations suggest that at least 90% mass of the Universe is due to some non-luminous matter, yet to be discovered, the so-called dark matter (DM). The term "dark matter" was coined by Zwicky in 1933 when he found some evidence about the missing mass in studying cluster of galaxies known as "Coma" [1]. He found that the expansion of the space (red-shift) in the Coma cluster could not be explained in terms of the known luminous mass. He applied the virial theorem and concluded that a large amount of dark matter must be present to keep these galaxies bound together. The measurements of the cosmic microwave background (CMB), too, suggest that dark matter is necessary to explain structure formation [2]. Structure formation implies that clumps of neutral particles arose through the gravitational attraction, form neutral atoms which were attracted gravitationally by dark matter to form the galaxies. Another evidence of dark matter is the high temperature of the gas detected in clusters through its X-ray emission [2, 3]. Currently there is a plethora of modern observations which support and confirm the existence of dark matter on a wide range of scales. Many DM candidates have been proposed and studied over the years by cosmologists and particle physicists alike in an effort to constrain its properties. For a nice list of the existing DM candidates see e.g. [4], and for DM searches go through Refs. [5–7]. Despite that, the origin and nature of DM still remains unknown. Indeed, the determination of the type of elementary particles that play the role of dark matter in the Universe is one of the current challenges of Particle Physics and modern Cosmology.

Weakly Interacting Massive Particles (WIMPs), which are thermal relics from the Big-Bang, are perhaps the most popular DM candidates. Initially, when the Universe was very hot, WIMPs were in thermal equilibrium with their surrounding particles. As the Universe expands and cools down, at a certain temperature which depends on the precise values of the mass of the DM particle and its couplings to the Standard Model (SM) particles, WIMPs decouple from the thermal bath, and its abundance freezes out. After freezing out, they can no longer annihilate, and their density is the same since then comprising the observed DM abundance of the Universe [2]. If WIMPs, or neutralinos in particular, are the main candidates for DM, they will cluster gravitationally with stars, and also form a background density in the Universe. In Ref. [8], it was remarked that our own galaxy, the Milky Way, contains a large amount of dark matter. This raises the hope of detecting relic WIMPs directly, by scattering experiments in Earth-based detectors. The interaction of the neutralino with nuclei through elastic [2] or inelastic scattering [9, 10] is being studied in various laboratories. More than 20 experiments worldwide for DM direct detection are either running or in preparation, and some of them are the following: the DArk MAtter (DAMA) experiment [11, 12], Cryogenic Dark Matter Search (CDMS) experiment [13], EDELWEISS experiment [14], IGEX [15], ZEPLIN [16], GErmanium DEtectors in ONe cryostat (GEDEON) [17], CRESST [18], GErmanium in liquid NItrogen Underground Setup (GENIUS) [19], and LHC. Furthermore, Fermi LAT, GAMMA-400, IceCube, Kamiokande, and AMS-02 are some of the indirect DM detection experiments [6].

The null results of the rest of the DM direct detection experiments [20] and the recently discovered channelling effect on the threshold energy in DAMA give a spin independent (SI) cross section of elastic scattering of DM with nuclei in the range [21, 22]

$$3 \times 10^{-41} cm^2 \lesssim \sigma_p^{SI} \lesssim 5 \times 10^{-39} cm^2 \tag{1}$$

while the range of the mass of the DM particle is

$$3GeV \lesssim m_{DM} \lesssim 8GeV. \tag{2}$$

Various studies have taken these results into account [23–26]. In the WIMP scenario, a one-to-one relation is seen between the SI direct detection rate and DM relic density if its elastic scattering on nuclei occurs dominantly through Higgs exchange [21]. The SI direct detection cross section of elastic scattering of DM with nuclei is given by [21]

$$\sigma(\Psi N \to \Psi N) = \frac{y^2}{\pi}\frac{\mu_r^2}{v^2 M_h^4} f^2 m_N^2, \tag{3}$$

where $v = 246\ GeV$ is the Higgs vacuum expectation value, m_N, M_h are the nucleon mass and the Higgs mass, respectively, y, fm_N/v are the Yukawa couplings for DM interaction with Higgs boson and the interaction of Higgs particle with the nucleons, respectively. Finally, $\mu_r = \frac{m_N m_{DM}}{m_N + m_{DM}}$ is the reduced mass of a nucleon-DM particle system. The variables of Eq. 3 are determined within the Next-to- Minimal Supersymmetric Standard Model (NMSSM) [27], provided the maximum value of spin independent cross section (Eq. 1). In this work, we explore the consequences of the existence of DM particle (within NMSSM) in a very different environment, namely a neutron star.

Neutron stars (NS) are considered to be unique cosmic laboratories to explore properties of ultra dense matter under extreme conditions of density and neutron-proton asymmetry. Neutron stars are one of the remnants of dead stars having mass between $1.4 - 3.0 M_\odot$, undergoing gravitational collapse. The mass of a NS is dominated by the core contribution. Due to their wonderful nature, neutron stars are called "superstars". The historical first detection of gravitational waves (GW170817) from the binary neutron-star (BNS) merger by the LIGO-Virgo collaboration [28] has opened a new dimension in the fields of astrophysics, cosmology, gravitational physics, and fundamental physics. GW170817 observation suggests that the mass and radius of a NS lie in the range $2.01 \pm 0.04 \lesssim M(M_\odot) \lesssim 2.16 \pm 0.03$ [29] and $8.7 < \hat{R}$(km) 14.1 to a 90% confidence limit [30], respectively. The properties of NSs are predicted by its equation-of-state (EOS), a certain relation between energy density and pressure. EOSs are used in the Tolman-Oppenheimer-Volkoff (TOV) equations [31] to study the mass-radius relation and other physical quantities of NS. On the otherhand, by measuring the mass and radius of NSs (pulsars), its EOS can be constrained. Moreover, the tidal deformability Λ of NS from the GW170817 data [28] provides a new probe to the interior of NSs and their nuclear EOS [32]. It was pointed out in [33] that the mass-radius relation of NS can be affected in the presence of DM inside the object. What is more, the presence of DM inside NSs can modify the gravitational waves (GWs) signal from BNS merger which may result in yielding an additional peaks in the post-merger frequency spectrum [34]. These peaks might be detected in future GW signal from BNS mergers. Therefore, the detection of such additional peaks can be an indirect tool to detect DM.

The consequences of DM inside NSs have been discussed in the literature [34–42]. These discussions include the effect of charged massive dark matter particle on NSs [37], trapped WIMPs inside the neutron star [38], dark matter annihilation and its effect on NS [39–41], or the collapse of a neutron star due to accretion of non annihilating dark matter [42] etc. The effects of a self-interacting DM core on the maximum mass, radius and tidal deformability of NSs have been studied in [34, 35] assuming different nuclear EOSs as well as different fractions of DM. In [43], the authors studied the properties of NSs considering the DM halo and constrained the DM parameters using the GW170817 data. The authors of [33, 44], in the framework of relativistic mean field (RMF) theory, considered the Walecka model [45–48] for the nucleonic part and fermionic dark matter inside the neutron star with additional self-coupling of Higgs boson in Ref. [33]. They considered the Standard Model Higgs boson in their study. The key point is that the properties of NSs (more specifically Λ) decrease in the case of DM core [33, 44], whereas Λ increases in the DM halo model of [43]. In this manuscript, we have examined the effects of DM core inside a NS with the parameters of DM within the NMSSM model. We have considered the effective field theory motivated relativistic mean field field model (E-RMF) to generate the EOS of NS by considering the IOPB-I [49], G3 [50], and NL3 [51] parameter sets.

The paper is organized as follows: The formalism adopted in this work is presented in Sec. II. In the sub-section II A we briefly present the E-RMF formalism with the EOS of nuclear matter for the parameters chosen. The sub-section II B contains the full Lagrangian with the inclusion of DM in NSs, while in the Sub-section II C the TOV equations together with the observables studied here are presented. Our numerical results are discussed in Sec. III. Finally, we summarize and conclude our work in Sec. IV.

II. FORMALISM

A. Effective field theory motivated relativistic mean field model (E-RMF)

The relativistic mean field (RMF) theory is one of the widely used microscopic approaches to investigate the properties of nuclear system, i.e., from finite nuclei to nuclear matter. In the RMF model nucleons interact through the exchange of mesons, which modify the nucleon bare properties. Thus they are quasi-particles with medium-dependent effective mass and baryon chemical potential. The advantage of RMF over its non-relativistic counterpart is that it accounts for spin orbit interaction automatically. The E-RMF model is nothing but the extension of simple RMF in which all possible types of mesons and their self and cross coupling are considered. In this work we have used the E-RMF Lagrangian, including contributions from $\sigma-$, $\omega-$ mesons with powers up to 4^{th} order, and $\rho-$ and $\delta-$ mesons with powers up to 2^{nd} order, which has been shown to be a good approximation to predict observables of nuclear systems in a considerably satisfactory way [49, 52]. The details of the E-RMF formalism can be found in [49, 52, 53]. Here, for the sake of completeness, we present the energy density and pressure for the considered hadronic Lagrangian density ($\mathcal{L}_{had.}$).

The temporal ($< T_{00} >$) and spatial ($< T_{ii} >$) components of the energy-momentum tensor $< T_{\mu\nu} >$ [54] give the en-

ergy density and pressure of a system, respectively [55]. By applying the mean field approximations, the energy density for infinite nuclear matter within E-RMF is:

$$\begin{aligned}\mathcal{E}_{had.} &= \frac{2}{(2\pi)^3}\int d^3k E_i^*(k) + \rho_b W + \frac{m_s^2\Phi^2}{g_s^2}\left(\frac{1}{2}+\frac{\kappa_3}{3!}\frac{\Phi}{M}+\frac{\kappa_4}{4!}\frac{\Phi^2}{M^2}\right)\\ &-\frac{1}{2}m_\omega^2\frac{W^2}{g_\omega^2}\left(1+\eta_1\frac{\Phi}{M}+\frac{\eta_2}{2}\frac{\Phi^2}{M^2}\right)-\frac{1}{4!}\frac{\zeta_0 W^4}{g_\omega^2}+\frac{1}{2}\rho_3 R\\ &-\frac{1}{2}\left(1+\frac{\eta_\rho\Phi}{M}\right)\frac{m_\rho^2}{g_\rho^2}R^2-\Lambda_\omega(R^2\times W^2)+\frac{1}{2}\frac{m_\delta^2}{g_\delta^2}\left(D^2\right), \end{aligned} \tag{4}$$

while the pressure for infinite nuclear matter is given by,

$$\begin{aligned}P_{had.} &= \frac{2}{3(2\pi)^3}\int d^3k\frac{k^2}{E_i^*(k)} - \frac{m_s^2\Phi^2}{g_s^2}\left(\frac{1}{2}+\frac{\kappa_3}{3!}\frac{\Phi}{M}+\frac{\kappa_4}{4!}\frac{\Phi^2}{M^2}\right)\\ &+\frac{1}{2}m_\omega^2\frac{W^2}{g_\omega^2}\left(1+\eta_1\frac{\Phi}{M}+\frac{\eta_2}{2}\frac{\Phi^2}{M^2}\right)+\frac{1}{4!}\frac{\zeta_0 W^4}{g_\omega^2}\\ &+\frac{1}{2}\left(1+\frac{\eta_\rho\Phi}{M}\right)\frac{m_\rho^2}{g_\rho^2}R^2+\Lambda_\omega(R^2\times W^2)-\frac{1}{2}\frac{m_\delta^2}{g_\delta^2}\left(D^2\right), \end{aligned} \tag{5}$$

where Φ, D, W, and R are the redefined fields for σ, δ, ω, and ρ mesons as $\Phi = g_s\sigma$, $D = g_\delta\delta$, $W = g_\omega\omega^0$, and $R = g_\rho\bar{\rho}^0$, respectively, while $E_i^*(k)$=$\sqrt{k^2+M_i^{*2}}$ $(i = p, n)$ is the energy with effective mass $M_i^{*2} = k_F^2 + M_i^2$, and k is the momentum of the nucleon. The quantities ρ_b and ρ_3 in Eq. 4 are the baryonic and iso-scalar densities as defined in [49].

B. Equation of state for neutron star in the presence of dark matter

We have considered the lightest mass eigenstate of WIMP, i.e. neutralino (χ) within NMSSM as the fermionic DM candidate. We assume that DM particles do not interact with the nucleonic matter directly. Rather, they couple to Higgs field h, which mediates the interaction with baryonic matter. In the presence of DM, the interaction Lagrangian density is given by [44]

$$\begin{aligned}\mathcal{L} &= \mathcal{L}_{had.} + \bar{\chi}\left[i\gamma^\mu\partial_\mu - M_\chi + yh\right]\chi + \frac{1}{2}\partial_\mu h\partial^\mu h\\ &-\frac{1}{2}M_h^2h^2 + f\frac{M_n}{v}\bar{\varphi}h\varphi, \end{aligned} \tag{6}$$

where $\mathcal{L}_{had.}$ is the Lagrangian density for pure hadronic matter. We have not considered the higher order terms of the Higgs scalar potential (*i.e.*, h^3 and h^4), since in the mean field theory approximation these terms are negligible [33].

The factor f parameterizes the Higgs-nucleon coupling, and a complete expression for f can be found in [56]. Following the lattice computations [57–59], we shall consider the central value $f = 0.3$ in agreement with [56]. For the DM sector, we shall assume a mass range and a SI DM-nucleon cross section suggested by the DAMA results [11, 12]. It is easy to verify that if we take the Higgs mass to be 125 GeV, the Yukawa coupling y computed using Eq. 3 lies in the non-perturbative regime. Therefore we have to assume a light Higgs boson with a mass $M_h = 40\ GeV$, so that $y < 1$. The authors of [27, 60] have shown that such a scenario can be realized in the framework of the NMSSM in agreement with the rest of the experimental constraints.

The NMSSM [61–63] (for a review see [64]) is a simple extension of the MSSM in which a singlet supermultiplet is added, and it is characterized by the following properties: i) It preserves the nice properties of the MSSM, i.e. it solves the hierarchy problem while at the same time it provides us with an excellent DM candidate, ii) it solves the μ problem [65], and iii) there is a rich Higgs sector with 2 Higgs bosons

more in comparison with MSSM. In particular, if some of the Higgs bosons have a significant singlino component they can be light, $M_H \leq 70\, GeV$, without any contradiction to experimental constraints [66]. As a matter of fact, it has been shown that in NMSSM it is possible to obtain a DM-nucleon spin-independent cross section as high as the one indicated by the DAMA results, precisely due to the exchange of light Higgs bosons, which cannot be achieved in the MSSM [27, 60].

Solving the full Lagrangian density (Eq. 6) by the variational principle, and taking care of all the mean field and infinite nuclear matter approximations [44, 49], the energy density and pressure are given by

$$\mathcal{E} = \mathcal{E}_{had.} + \frac{2}{(2\pi)^3}\int_0^{k_F^{DM}} d^3k\sqrt{k^2+(M_\chi^\star)^2} + \frac{1}{2}M_h^2 h_0^2. \quad (7)$$

$$P = P_{had.} + \frac{2}{3(2\pi)^3}\int_0^{k_F^{DM}} \frac{d^3k k^2}{\sqrt{k^2+(M_\chi^\star)^2}} - \frac{1}{2}M_h^2 h_0^2. \quad (8)$$

The Fermi momentum of DM particles (k_f^{DM}) is taken to be a constant throughout the calculation with the value fixed at 0.06 GeV. However, in Refs. [33, 44], authors vary its value in the particular range. The effective mass of the nucleon (M^*) is modified due to the interaction with the Higgs boson. The new effective mass of the nucleon $M^\star$ and the effective mass of the DM particle $M_\chi^\star$ are given by,

$$\begin{aligned} M_i^\star &= M_i + g_\sigma\sigma - \tau_3 g_\delta\delta - \frac{f M_n}{v}h_0, \\ M_\chi^\star &= M_\chi - y h_0. \end{aligned} \quad (9)$$

So far the discussion on the EOS has been for infinite nuclear matter. Now we present in the discussion to follow how to obtain the EOS for NSs. In a neutron star, the Fermi momentum of neutrons and proton are different due to the different number densities of these particles. The matter inside NSs is mainly composed of neutrons, which eventually decay to protons as,

$$\begin{aligned} n &\rightarrow p + e^- + \bar{\nu}, \\ n + \nu &\rightarrow p + e^-. \end{aligned} \quad (10)$$

For the stability of NSs, the $\beta-$ equilibrium condition is imposed, which is given by,

$$\begin{aligned} \mu_n &= \mu_p + \mu_e, \\ \mu_e &= \mu_\mu. \end{aligned} \quad (11)$$

where, μ_n, μ_p, μ_e, and μ_μ are the chemical potentials of neutrons, protons, electrons, and muons, respectively. The muon comes into play when the chemical potential of the electrons reaches the muon rest mass and maintains the charge of NS as follows

$$\rho_p = \rho_e + \rho_\mu. \quad (12)$$

The chemical potentials μ_n, μ_p, μ_e, and μ_μ are given by,

$$\mu_n = g_\omega\omega_0 + g_\rho\rho_0 + \sqrt{k_n^2+(M_n^\star)^2}, \quad (13)$$

$$\mu_p = g_\omega\omega_0 - g_\rho\rho_0 + \sqrt{k_p^2+(M_p^\star)^2}, \quad (14)$$

$$\mu_e = \sqrt{k_e^2+m_e^2}, \quad (15)$$

$$\mu_\mu = \sqrt{k_\mu^2+m_\mu^2}. \quad (16)$$

The particle fraction is determined by the self-consistent solution of Eq. 11 and Eq. 12 for a given baryon density. The total energy density and pressure for $\beta-$ stable NS are given by,

$$\begin{aligned} \mathcal{E}_{NS} &= \mathcal{E} + \mathcal{E}_l \\ P_{NS} &= P + P_l. \end{aligned} \quad (17)$$

Where,

$$\mathcal{E}_l = \sum_{l=e,\mu}\frac{2}{(2\pi)^3}\int_0^{k_l} d^3k\sqrt{k^2+m_l^2}, \quad (18)$$

and

$$P_l = \sum_{l=e,\mu}\frac{2}{3(2\pi)^3}\int_0^{k_l}\frac{d^3k k^2}{\sqrt{k^2+m_l^2}} \quad (19)$$

are the energy density and pressure for leptons (e and μ). The EOSs of NS (Eq. 17) are used as the input (with the representation $\mathcal{E}_{NS} \equiv \mathcal{E}$ and $P_{NS} \equiv P$) to TOV equations to find the NS observables.

C. Mass, radius, tidal deformability, and moment of inertia of NS

The structural properties, such as the mass-to-radius profile, the tidal deformability, the moment of inertia $etc.$, are studied in this work. Given an EOS it is straightforward to calculate the mass and radius of the NS by using the TOV equations [31]. For static, spherically symmetric solutions of the form $ds^2 = -e^{\nu(r)}dt^2 + e^{\lambda(r)}dr^2 + r^2d\theta^2 + r^2\sin^2\theta d\phi^2$, the TOV equations are given by,

$$e^{\lambda(r)} = \left(1 - \frac{2m(r)}{r}\right)^{-1}, \quad (20)$$

$$\frac{d\nu}{dr} = 2\,\frac{m+4\pi p r^3}{r(r-2m)}, \quad (21)$$

$$\frac{dp}{dr} = -\frac{(\mathcal{E}+p)(m+4\pi r^3 p)}{r(r-2m)}, \quad (22)$$

$$\frac{dm}{dr} = 4\pi r^2 \mathcal{E}. \tag{23}$$

The moment of inertia (MI) of NSs is obtained by solving the TOV equations along with the equation including the rotational frequency (given below). For a slowly rotating NS the MI is given by [67, 68],

$$I = \frac{8\pi}{3}\int_0^R r^4(\mathcal{E}+p)e^{(\lambda-\nu/2)}\frac{\bar{\omega}}{\Omega}dr, \tag{24}$$

where Ω and $\bar{\omega}$ are the angular velocity and the rotational drag function, respectively, for a uniformly rotating NS. The rotational drag function $\bar{\omega}$ meets the boundary condition,

$$\bar{\omega}(r=R) = 1 - \frac{2I}{R^3}, \qquad \frac{d\bar{\omega}}{dr}|_{r=0} = 0 \tag{25}$$

The quantity $\frac{\bar{\omega}}{\Omega}$, evolve in Eq. 24, is the dimensionless frequency satisfying the equation

$$\frac{d}{dr}\left(r^4 j\frac{d\bar{\omega}}{dr}\right) = -4r^3\bar{\omega}\frac{dj}{dr}, \tag{26}$$

with $j = e^{-(\lambda+\nu)/2}$.

The tidal deformability of a NS is one of the most important measurable physical quantities. It characterize the degree of deformation of NS due to the tidal field of its companion in BNS. During the last stage of NS binary, each component star of binary system develop a mass quadrupole due to the the tidal gravitational field of the partner NS. The tidal deformability for $l = 2$ quadrupolar perturbations is defined as,

$$\lambda_2 = \frac{2}{3}k_2 R^5, \tag{27}$$

where R is the NS radius, and k_2 is the tidal love number which depends on stellar structure. The k_2 is calculated using the expression [69],

$$\begin{aligned} k_2 = {} & \frac{8C^5}{5}(1-2C)^2(2(1-C)+(2C-1)y_R)\times \\ & \{4C^3\left(13-11y_R+2C^2(1+y_R)+C(-2+3y_R)\right) \\ & +2C\left(6-3y_R+3C(5y_R-8)\right)+3(1-2C)^2 \\ & \times(2+2C(y_R-1)-y_R)\log(1-2C)\}^{-1}, \end{aligned} \tag{28}$$

where $C = M/R$ is the compactness of the NS, and $y_R = y(R)$ is obtained by solving the following differential equation

$$r\frac{dy}{dr} + y^2 + yF(r) + r^2 Q(r) = 0 \tag{29}$$

with

$$\begin{aligned} F(r) &= \frac{r-4\pi r^3(\mathcal{E}-p)}{r-2M}, \\ Q(r) &= \frac{4\pi r\left(5\mathcal{E}+9p+\frac{\mathcal{E}+p}{\partial p/\partial\mathcal{E}}-\frac{6}{4\pi r^2}\right)}{r-2M} \\ & \quad -4\left[\frac{M+4\pi r^3 p}{r^2(1-2M/r)}\right]^2, \end{aligned} \tag{30}$$

along with the TOV equations (20, 21,22, and 23) with the appropriate boundary conditions, as given in [44]. After solving these equations and obtaining the values M, R, k_2 *etc.*, one can compute the dimensionless tidal polarizability as: $\Lambda = 2/3k_2 C^{-5}$.

III. RESULTS AND DISCUSSIONS

A. Effect of dark matter on the EOS of neutron star

The main goal of this work is to investigate the effects of the DM core on the properties of NSs, which depend entirely on the nature of the EOS of the object. We have obtained the EOSs within E-RMF model using recently developed parameter sets, such as IOPB-I [49] and G3 [50]. The merit of these parameter sets is that they pass through or relatively close to the low as well as high density region [49]. The EOS corresponding to the G3 set is softer than the one corresponding to the IOPB-I parameter set [49]. For comparison reasons, we also consider the NL3 parameter set [51], which is one of the best known and widely used set. The EOS corresponding to the NL3 set is the stiffest among the chosen parameter sets. Table I shows the values of the coefficients of Eqs. 4, 5 for the parameters sets considered here. To obtain the EOS of the NS in the presence of DM, we need the values of the parameters for the DM part in the full Lagrangian (Eq. 6). The values of the quantities involved in Eq. 6 have been already mentioned in the sub-section II B except M_χ and the Yukawa coupling y. It has been stated that the y values are obtained using Eq. 3, varying the mass of the DM particle in the range specified in Eq. 2.

In Figure 1, the EOSs of NSs corresponding to the G3, IOPB-I, and NL3 parameter sets are shown for two different values of DM particle mass i.e., $M_{DM} = 4$ GeV (dashed curve) and $M_{DM} = 8$ GeV (dash-dotted curve). For comparison reasons, the EOSs without dark matter $M_{DM} = 0$ GeV (bold curves) are also shown for all the parameter sets. The grey and yellow shaded regions represent the 50% and 90% confidence level of EOS, obtained from GW data [70]. This was done using the spectral EOS parameterization with the condition that the EOS must support at least a 1.97 $M_\odot$ star [70]. In this way, the pressure posterior band [70] shrinks about three times from the prior pressure [28] (not shown here). It is remarked in [70] that posterior EOS becomes softer than the prior EOS. The vertical lines (blue lines) represent the nuclear saturation density and twice its value. These densities are assumed to almost correlate with bulk macroscopic properties of NSs [71]. The pressure at twice of the nuclear saturation density is measured to be $21.88^{+16.88}_{-10.62}$ MeV-fm^{-3} [70]. We see that the presence of DM inside NSs softens the EOS. Large mass of DM particle has more impact in softening the EOS. For the G3 EOSs, the effect of DM is insignificant, while for the other two sets, the shift of the curves with the increase of the mass of the DM particle can be easily seen. It can be observed from the figure that G3 and IOPB-I EOSs with and without DM pass through the 90% credible limit of experimental band (posterior EOS) at and around the

TABLE I: The parameters involved in EOS (Eqs. 4, 5) corresponding to IOPB-I [49], G3 [50], and NL3 [51] parameter sets are listed. The mass of nucleon M is 939.0 MeV in all the sets. All the coupling constants are dimensionless, except k_3 which is in fm^{-1}.

	NL3	G3	IOPB-I
m_s/M	0.541	0.559	0.533
m_ω/M	0.833	0.832	0.833
m_ρ/M	0.812	0.820	0.812
m_δ/M	0.0	1.043	0.0
$g_s/4\pi$	0.813	0.782	0.827
$g_\omega/4\pi$	1.024	0.923	1.062
$g_\rho/4\pi$	0.712	0.962	0.885
$g_\delta/4\pi$	0.0	0.160	0.0
k_3	1.465	2.606	1.496
k_4	-5.688	1.694	-2.932
ζ_0	0.0	1.010	3.103
η_1	0.0	0.424	0.0
η_2	0.0	0.114	0.0
η_ρ	0.0	0.645	0.0
Λ_ω	0.0	0.038	0.024

nuclear saturation density ρ_{nucl}. These EOSs pass through the 50% confidence level too at slightly larger energy density than ρ_{nucl}, while at larger nuclear density, these EOSs become softer than the shaded band. However, NL3 EOSs satisfy the 90% as well as 50% confidence level of posterior EOSs only at a very large value of the energy density. The effects of the DM core on the EOSs are consistent with what was obtained in [33, 44], where the authors fixed the mass of DM particle and varied the wave number of the DM particle. In [33, 44], the effects of DM were larger due to the fact that there the SM Higgs boson was the mediator. In this work, however, we have considered lighter DM particle and Higgs boson within the NMSSM model, as mentioned above, which can accommodate for scattering results consistent with the DAMA experiment. It is important to mention that the EOS becomes stiffer when considering the DM haloes around NS [43]. In this case, an enhancement in structural properties is reported in [43]. The softening of EOS in the presence of the DM core is supported by the posterior EOS, which describes the structure of NS with mass at least 1.97 $M_\odot$.

B. Neutron star observables

The mass-radius relation for NSs is presented in Figure 2 using the EOSs as shown in Figure 1. The violet band represents the maximum mass range for a non-rotating NS, which is constrained through GW170817 data and lie in the range $2.01 \pm 0.04 \lesssim M(M_\odot) \lesssim 2.16 \pm 0.03$ [29]. This band

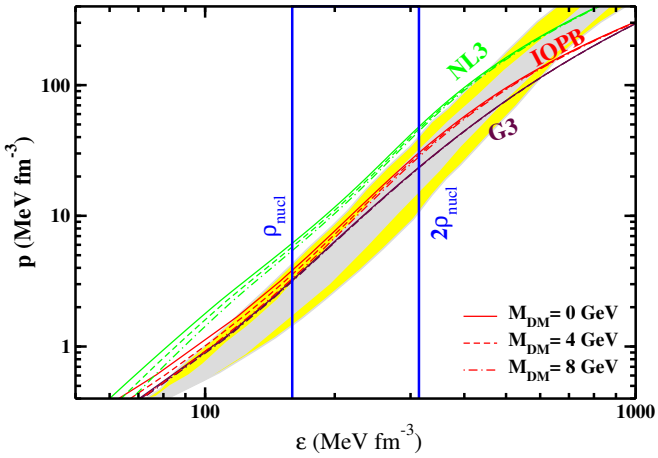

FIG. 1: (color online) The EOSs of NS in the presence of DM, corresponding to G3, IOPB-I, and NL3 parameter sets. The bold line labelled as $M_{DM} = 0$ GeV represent the EOSs without considering DM. The dashed and dash-dotted line represent the EOSs in the presence of DM with the neutralino mass $M_{DM} = 4$ GeV and $M_{DM} = 8$ GeV, respectively. The grey (yellow) shaded region correspond to the 50% (90%) posterior credible limit from the GW data [70].

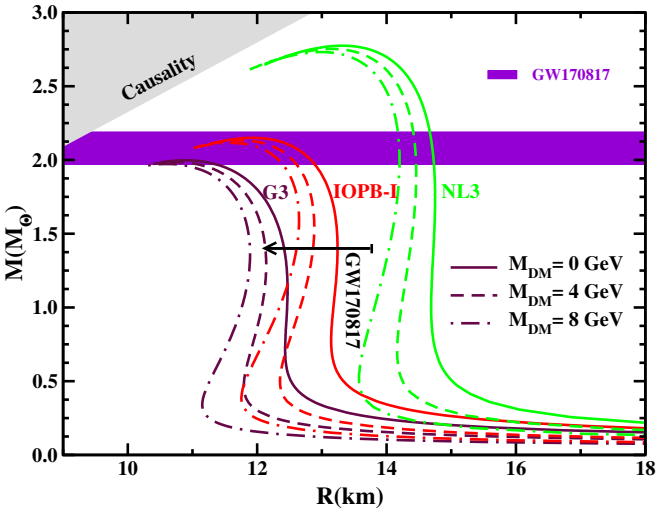

FIG. 2: (color online) The mass-radius relation for NS in the presence of DM core corresponding to the IOPB-I [49], G3 [50], and NL3 [51] parameter sets. The recent constraints on the mass [29] and radii [73] of NS are also shown. The grey shaded region shows the causality region [74].

also satisfies the precisely measured mass of NS, such as PSR J0348+0432 with mass $(2.01 \pm 0.04)M_\odot$ [72]. These results imply that the theoretically predicted masses of NSs should reach the limit $\sim 2.0\ M_\odot$. The black arrow represents the radius at the canonical mass of NS [73] with the maximum value $R_{1.4} \leq 13.76$ km. As anticipated, the mass-radius (MR) curves go down in the presence of a DM core. The small effect of the DM core on the G3 EOS also produces a significant shift of the MR curve to the left with a slightly lower highest mass. The bold, dashed, and dash-dotted lines correspond to

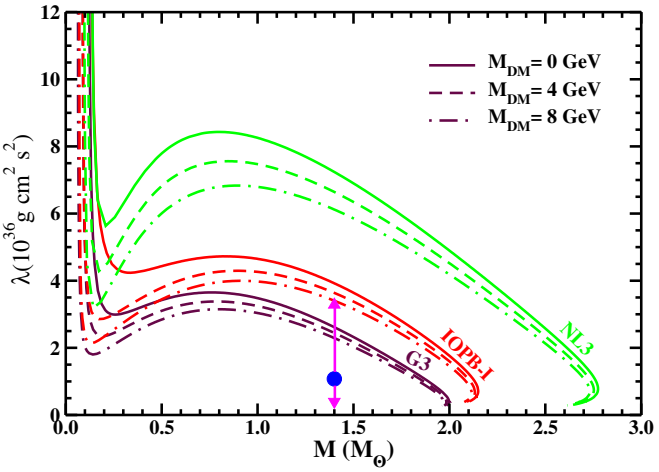

FIG. 3: (color online) Tidal deformability λ_2 as a function of NS mass corresponding to the IOPB-I, G3, and NL3 EOSs. The dashed and dash-dotted line represent the EOSs in the presence of DM with the neutralino mass $M_{DM} = 4$ GeV and $M_{DM} = 8$ GeV, respectively. The blue circle with the arrow bar represent the λ_2 value at $1.4M_\odot$ NS mass obtained from GW data [70].

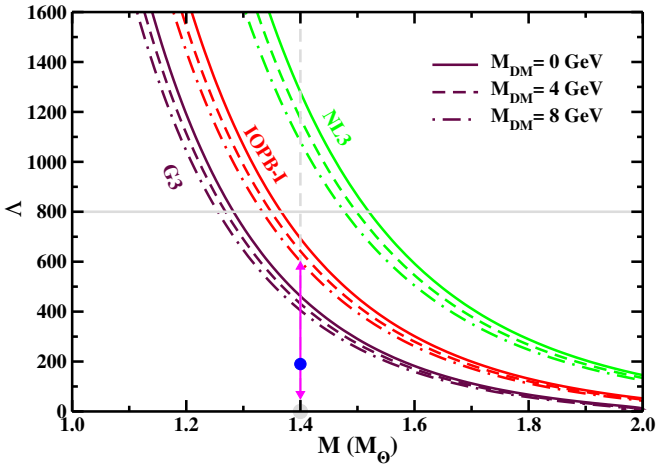

FIG. 4: (color online) The dimensionless tidal deformability parameter (Λ) as a function of NS mass corresponding to the IOPB-I, G3, and NL3 EOSs. The dashed grey line represent the canonical mass of NS. However, the bold grey line shows the upper limit of Λ value from GW170817 data [28]. The blue circle with the error bar represent the $\Lambda_{1.4}$ value for posterior GW170817 data [70].

the same representation throughout this work, as mentioned for EOS figure (Fig. 1). The NL3 set, being the stiffest among the considered parameter sets, predicts large mass and radius. The G3 and IOPB-I EOSs with a DM core predict the maximum masses of NS that satisfy the mass range constrained in [29] from the prior GW data [28], while GW170817 data rule out the NL3 EOSs. On considering the large value of DM wave number, the EOSs for the NL3 set can be significantly reduced to satisfy the GW170817 mass range. In the figure, the lowering in the maximum mass of NS for the EOSs with DM is small. The effects of DM are more important for masses below the highest mass. In other words, the radius is reduced much at a fix mass other than the maximum masses. To be more specific, the radii corresponding to the canonical mass and the chirp mass of the NS binary are affected more by the DM core. Out of the three considered parameter sets, the IOPB-I EOSs with and without DM satisfy the radius range at canonical mass constrained from GW170817 [73]. The reduction in the chirp mass in the presence of the DM core may result in some additional peaks in the frequency curve of gravitational waves, and can be detected in near future.

The tidal deformability of NS depends on its mass quadrupole which is developed due to the tidal gravitational field of other component of NS binaries, as discussed above. It quantifies mainly the surface part of NS. We have calculated the tidal polarizability for $l = 2$ perturbation, i.e., λ_2. Recently, tidal deformability was discussed for the GW170817 data [28]. It is clear from its definition (Eq. 27) that λ_2 depends on the radius of the star and on its tidal love number k_2, which describes the internal structure of NS. As the radius of NS increases, λ_2 values grow, and the surface becomes more deform. It simply means that soft EOSs predict less value for λ_2. In Figure 3, we plot λ_2 for the chosen EOSs with and without DM. The blue circle with the arrow bar (error bar) represents the λ_2 of a NS at the mass $1.4M_\odot$ corresponding to the $\hat{\Lambda}_{1.4} = 190^{+390}_{-120}$, which is constrained from the GW data [70] at 90% confidence level. The NL3 set, which is stiffer, predicts large values for the tidal deformability and hence large deformation. The λ_2 corresponding to the NL3 EOSs, even in the presence of DM, does not pass through the experimental range at the canonical mass. On the other hand, λ_2 curves for the G3 EOSs lie within the observationally allowed region. However, the IOPB-I EOS at neutralino mass $M_{DM} = 8$ GeV predicts a λ_2 value than just satisfies the upper range of the experimental λ_2 value. The shift of the curves for λ_2 versus the mass of NSs can be easily noticed from the figure. The significant changes occur in λ_2 due to the DM core at the canonical mass of NS. The softening of EOS in the presence of the DM core, and hence, a lower λ_2 are supported by GW170817 data. We also show the dimensionless tidal deformability (Λ) of a single NS in Figure 4. The blue circle represents Λ at the canonical mass of NS from GW170817 posterior data [70], the numerical value of which is given above.

In Figure 5 we display the dimensionless tidal deformabilities Λ_1 and Λ_2 of a binary NS (BNS) corresponding to the G3, IOPB-I, and NL3 parameter sets. Here, we consider the tidal deformability constraint from GW170817 observation on EOSs of NSs in the presence of DM core. The individual dimensionless tidal deformabilities Λ_1 and Λ_2 correspond to high mass m_1 and low mass m_2 of BNS. We vary the mass m_1 in the range $1.365 < m_1/M_\odot < 1.60$, and determine the range of m_2 by fixing the chirp mass as $\mathcal{M}_c = 1.188\ M_\odot$. It can be seen in the figure that the G3 and IOPB-I sets are in excellent agreement with the 90% (bold line) and 50% (dashed line) probability contour of prior GW170817, shown by orange curves [28]. We also show the recently re-analyzed results of GW170817 data in magenta color [70]. The figure shows that only the curve corresponding to the G3 EOS, with

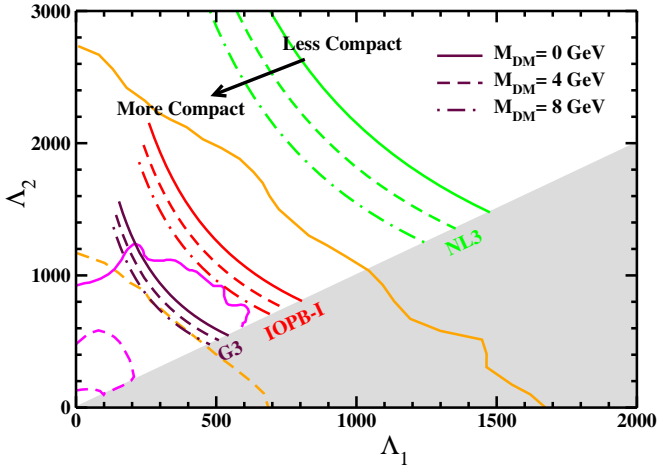

FIG. 5: (color online) Dimensionless tidal deformability Λ generated by using IOPB-I, G3, and NL3 EOSs with and without considering DM core. The calculated values are compared with 50% as well as 90% probability contour as given in GW170817 [28, 70] for the case of low spin, $|\chi| \leq 0.05$.

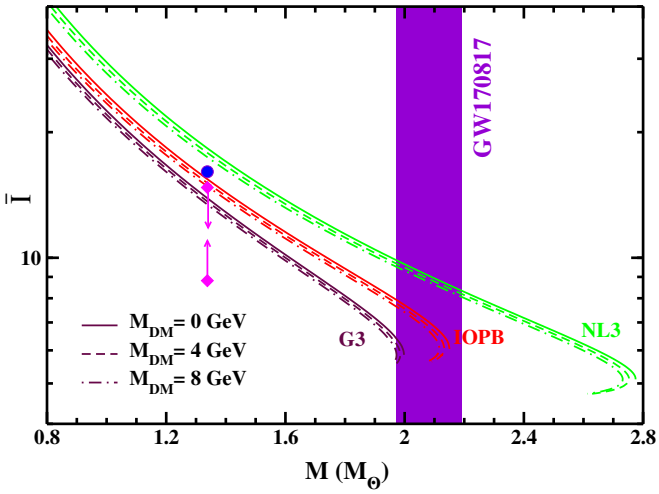

FIG. 6: (color online) The dimensionless moment of inertia $\bar{I}$ as a function of NS mass for EOSs shown in Fig. 1. The overlaid arrows represent the constraints on MI of PSR J0737-3039A set [78] from the analysis of GW170817 data [70]. The circle shows the upper bound from the minimal-assumption analysis of Ref. [28]. From reference point of view, the mass range of NS, constrained from GW data [29], is also shown by the violet band.

and without DM, lies within the 50% and 90% confidence level allowed region of prior as well as posterior GW170817 data. The $\hat{\Lambda}_{1.4} = 190^{+390}_{-120}$ has been found in [70] at 90% confidence level by imposing the condition of maximum mass at least 1.97 $M_\odot$ and assuming the same EOSs for both objects in the binaries. The shaded part (grey color) in the figure marks the $\Lambda_2 < \Lambda_1$ region that is naturally excluded for a common realistic EOS [70]. The analysis of [70] suggests that soft EOSs, which predict lower values for Λ, are favoured over stiffer EOSs. For the EOSs corresponding to NSs with a DM core, the curves are shifted to the left and predict lower values for $\hat{\Lambda}$ corresponding to less compact NSs. The NL3 EOSs lie outside the 90% confidence lever region (bold line) of prior (orange) as well as posterior (magenta) analysis. The lowering of the tidal deformability parameter in the presence of the DM core is favoured by the GW constraints on $\hat{\Lambda}$. On adjusting the parameters of the DM Lagrangian for an EOS, the curve can be shifted even more to the left. In this way, the parameters of the DM Lagrangian can be optimized satisfying the GW170817 constraint.

The moment of inertia (MI) of NSs strongly depends on the structure of the object. For a spherically symmetric NS the moment of inertia is computed solving Eqs. 24, 25, and 26 together with the TOV equations. It is one of the most important macroscopic quantities that can be used to constrain the EOS of NSs. The MI of the binary pulsar, PSR J0737-3039, is expected to be determined within $\sim 10\%$ accuracy by measuring its angular momentum [75–77]. The mass distribution of NSs, the final stage of the BNS merger, and $r-$ process nucleosynthesis are determined by the EOS, and therefore a precise measurement of the MI, tidal deformability etc are very important. In Figure 6 we plot the dimensionless MI, which decreases with the mass of the NS. Stiffer EOSs predict a larger MI for a given mass of a NS. In the presence of a DM core, the soft nature of EOSs generates a lower MI. The overlaid arrows in the figure indicate the MI of PSR J0737-3039, constrained by the analysis of GW170817 [70], while the circle represents the upper bound on MI from minimal assumption analysis [28].

IV. SUMMARY AND CONCLUSIONS

In summary, we have analyzed the effect of a DM core on the properties of NSs. We have considered the lightest mass eigenstate of WIMP, i.e., neutralinos, which are trapped uniformly in the NS core. The neutralino interacts with baryonic matter through the exchange of the Higgs boson. The lightest CP-even eigenstate of the NMSSM has been taken as the mediator Higgs boson, because within NMSSM, scattering cross section of the DM particle with nuclei satisfies the DAMA results. The EOSs of NSs are generated using the E-RMF Lagrangian density including the interaction Lagrangian density of DM with baryonic matter, and applying the $\beta-$ equilibrium and charge neutrality conditions. Within E-RMF, we have used the recent parameter sets, such as G3 and IOPB-I, along with the older and widely accepted NL3 set. Out of the three EOSs considered here, G3 is the softest one, and predicts relatively small values of NS observables in agreement with the GW170817 results. We have observed that the presence of DM in NSs soften the EOS, which results in lowering the values of NS observables, such as mass, radius, tidal deformability, and even moment of inertia. We have imposed the constraints from GW170807 on the mass, λ_2 values, dimensionless tidal deformability Λ and MI of NSs. The effects of DM are small at the maximum values of NS mass for different EOSs, while its impact is more significant in the lower mass region than in the higher mass range. In particular, the chirp

mass is highly affected by DM, which may result in two or three additional peaks in the frequency curve of GWs. These additional peaks can be detected in near future, and so, NSs may be one of the finest indirect tools to detect DM.

Acknowledgments:

A. Q. would like to acknowledge DST-INSPIRE for providing the financial support in the form of fellowship and Institute of Physics, Bhubaneswar, for providing the hospitality during the work. G. P. thanks the Fundação para a Ciência e Tecnologia (FCT), Portugal, for the financial support to the Center for Astrophysics and Gravitation-CENTRA, Instituto Superior Técnico, Universidade de Lisboa, through the Grant No. UID/FIS/ 00099/2013. B. K. thanks the Navajbai Ratan Tata Trust for providing partial support for this work.

[1] F. Zwicky, Helv. Phys. Acta **6**, 110 (1933); Gen. Relativ. Gravit. **41**, 207 (2009).
[2] Carlos Muńoz, Int. Journal of Mod. Phys. A **19**, 3039, (2004).
[3] L. Bergstrom, M. Fairbairn, and L. Pieri, Phys.Rev. D **74**, 123515 (2006).
[4] M. Taoso, G. Bertone and A. Masiero, JCAP **0803**, 022 (2008) 022.
[5] J. Gascon, EPJ Web Conf. **95**, 02004 (2015).
[6] J. M. Gaskins, Contemp. Phys. **57**, 496 (2016); [arXiv:1604.00014 [astro-ph.HE]].
[7] F. Kahlhoefer, Int. J. Mod. Phys. A **32**, 1730006 (2017); [arXiv:1702.02430 [hep-ph]].
[8] P. F. Smith and J. D. Lewin, Phys. Rep. **187**, 203 (1990).
[9] J. Ellis, R. A. Flores and J. D. Lewin, Phys. Lett. B **212**, 375 (1988); H. Ejiri, K. Fushimi and H. Ohsumi, Phys. Lett. B **317**, 14 (1993).
[10] G. D. Starkman and D. N. Spergel, Phys. Rev. Lett. **74**, 2623 (1995).
[11] DAMA Collab. (R. Bernabei et al.), Phys. Lett. B **480**, 23 (2000).
[12] DAMA Collab. (R. Bernabei et al.), Riv. Nuovo Cimento **26**, 1 (2003).
[13] CDMS Collab. (R. Abusaidi et al.), Phys. Rev. Lett. **84**, 5699 (2000); D. Abrams et al., Phys. Rev. D **66**, 122003 (2002).
[14] EDELWEISS Collab. (A. Benoit et al.), Phys. Lett. B **513**, 15 (2001); A. Benoit et al., ibid. B **545**, 43 (2002).
[15] IGEX Collab. (A. Morales et al.), Phys. Lett. B **532**, 8 (2002).
[16] D. S. Akerib *etal*., arXiv:1509.02910 [physics.ins-det]; arXiv:1802.06039
[17] A. Morales, arXiv:hep-ex/0111089.
[18] CRESST Collab. (M. Bravin et al.), Astropart. Phys. **12**, 107 (1999); arXiv:hep-ex/9904005v1.
[19] GENIUS Collab. (H. V. Klapdor-Kleingrothaus et al.), arXiv:hep-ph/9910205.
[20] D. S. Akreib *etat*. [CDMS Collaboration], Phys. Rev. D **68**, 082002 (2003) [arXiv:hep-ex/0306001]; Z. Ahmed *etal*. [CDMS Collaboration], arXiv:0802.3530 [astro-ph]; D. S. Akerib *etal*. [CDMS Collaboration], Phys. Rev. Lett. **96**, 011302 (2006) [arXiv:astro-ph/0509259]; J. Angle *etal*. [XENON Collaboration], Phys. Rev. Lett. **100**, 021303 (2008) [arXiv:0706.0039 [astro-ph]].
[21] Sarah Andreas, Thomas Hambye, and Michel H. G. Tytgat, arXiv:0808.0255v2 [hep-ph].
[22] F. Petriello and K. M. Zurek, arXiv:0806.3989 [hep-ph].
[23] R. Foot, arXiv:0804.4518 [hep-ph].
[24] J. L. Feng, J. Kumar and L. E. Strigari, arXiv:0806.3746 [hep-ph].
[25] A. Bottino, F. Donato, N. Fornengo and S. Scopel, arXiv:0806.4099 [hep-ph].
[26] F. T. Avignone, R. J. Creswick and S. Nussinov, arXiv:0807.3758 [hep-ph].
[27] John F. Gunion, Alexander V. Belikov, and Dan Hooper, arXiv:1009.2555v1 [hep-ph].
[28] B. Abbott et al. (Virgo, LIGO Scientific), Phys. Rev. Lett. **119**, 161101 (2017), arXiv:1710.05832 [gr-qc].
[29] L. Rezzolla, Elias R. Most, and Lukas R. Weth, Astrophys. J. Lett. **852**, L25 (2018).
[30] S. De, D. Finstad, J. M. Lattimer, D. A. Brown, E. Berger, and C. M. Biwer, arXiv:1804.08583 [astro-ph.HE].
[31] J. R. Oppenheimer and G. M. Volkoff, Phys. Rev. 55, 374 (1939); R. C. Tolman, ibid. **55**, 364 (1939).
[32] E. Annala, T. Gorda, A. Kurkela, and A. Vuorinen, (2017), arXiv:1711.02644 [astro-ph.HE].
[33] G. Panotopoulos and I. Lopes, Phys. Rev. D **96**, 083004 (2017), arXiv:1709.06312 [hep-ph].
[34] J. Ellis, A. Hektor, G. Hutsi, K. Kannike, L. Marzola, M. Raidal, and V. Vaskonen, Phys.Lett. B **781**, 607 (2018).
[35] J. Ellis, G. Hutsi, K. Kannike, L. Marzola, M. Raidal, V. Vaskonen, Phys.Rev. D **97**, 123007 (2018).
[36] N. Raj, P. Tanedo, H.B. Yu, Phys. Rev. D **97**, 043006 (2018).
[37] A. Gould, B.T.Draine, R. W.Romani, and S. Nussinov, Phys. Lett. B. **238**, 337 (1990).
[38] I. Goldman, S. Nussinov, Phys.Rev. D **40**, 3221 (1989).
[39] C. Kouvaris, Phys.Rev. D **77**, 023006 (2008).
[40] C. Kouvaris, P. Tinyakov, Phys.Rev. D **82**, 063531 (2010).
[41] A. de Lavallaz and M. Fairbairn, Phys.Rev. D **81** 123521 (2010).
[42] T. Guver, A. E. Erkoca, M.H.Reno, and I. Sarcevic, JCAP **05**, 013 (2014).
[43] Ann Nelson, Sanjay Reddy, and Dake Zhou, arXiv:1803.03266v1 [hep-ph].
[44] Arpan Das, Tuhin Malik, and Alekha C. Nayak, arXiv:1807.10013v1 [hep-ph].
[45] J. D. Walecka, Ann. Phys. **83**, 491 (1974).
[46] B. D. Serot and J. D. Walecka, Int. J. Mod. Phys. E **6**, 515 (1997).
[47] Y.K. Gambhir, P. Ring, and A. Thimet, Ann. Phys. (N.Y.) **198**, 132 (1990).
[48] P. Ring, Prog. Part. Nucl. Phys. **37**, 193 (1996).
[49] Bharat Kumar, B. K. Agrawal and S. K. Patra, Phys. Rev. C **97**, 045806 (2018).
[50] Bharat Kumar, S. K. Singh, B. K. Agrawal, S. K. Patra, Nucl. Phys. A **966**, 197 (2017).
[51] G. A. Lalazissis, J. König and P. Ring, Phys. Rev. C **55**, 540 (1997).
[52] R. J. Furnstahl, B. D. Serot and H. B. Tang, Nucl. Phys. A **598**, 539 (1996); R. J. Furnstahl, B. D. Serot and H. B. Tang, Nucl. Phys. A **615**, 441 (1997).
[53] Abdul Quddus, K. C. Naik, and S. K. Patra, J. Phys. G: Nucl. Part. Phys. **45**, 075102 (2018).
[54] B. D. Serot and J. D. Walecka, Adv. Nucl. Phys. **16**, 1 (1986).
[55] S. K. Singh, S. K. Biswal, M. Bhuyan, and S. K. Patra, Phys. Rev. C **89**, 044001 (2014).
[56] J. M. Cline, K. Kainulainen, P. Scott and C. Weniger, Phys.

Rev. D **88** (2013) 055025 Erratum: [Phys. Rev. D **92** 039906 (2015)]; [arXiv:1306.4710 [hep-ph]].
[57] J. M. Alarćon, J. Martin Camalich and J. A. Oller, Annals Phys. **336**, 413 (2013); [arXiv:1210.4450 [hep-ph]].
[58] R. D. Young, PoS LATTICE **2012**, 014 (2012); [arXiv:1301.1765 [hep-lat]].
[59] L. Alvarez-Ruso, T. Ledwig, J. Martin Camalich and M. J. Vicente-Vacas, Phys. Rev. D **88**, 054507 (2013); [arXiv:1304.0483 [hep-ph]].
[60] K. J. Bae, H. D. Kim and S. Shin, Phys. Rev. D **82**, 115014 (2010); [arXiv:1005.5131 [hep-ph]].
[61] U. Ellwanger, M. Rausch de Traubenberg and C. A. Savoy, Phys. Lett. B **315**, 331 (1993); [hep-ph/9307322].
[62] U. Ellwanger, M. Rausch de Traubenberg and C. A. Savoy, Z. Phys. C **67**, 665 (1995); [hep-ph/9502206].
[63] U. Ellwanger, M. Rausch de Traubenberg and C. A. Savoy, Nucl. Phys. B **492**, 21 (1997); [hep-ph/9611251].
[64] M. Maniatis, Int. J. Mod. Phys. A **25**, 3505 (2010); [arXiv:0906.0777 [hep-ph]].
[65] J. E. Kim and H. P. Nilles, Phys. Lett. **138B**, 150 (1984).
[66] D. G. Cerdeno, C. Hugonie, D. E. Lopez-Fogliani, C. Munoz and A. M. Teixeira, JHEP **0412**, 048 (2004); [hep-ph/0408102].
[67] J. B. Hartle, Astrophy. J. **150**, 1005 (1967).
[68] J. M. Lattimer and M. Prakash, Astrophys. J. **550**, 426 (2001).
[69] T. Hinderer, Astrophys. J. **677**, 1216 (2008); **697**, 964(E) (2009).
[70] P. B. Abbott *et. al.*, arXiv:1805.11581 (2018) [gr-qc].
[71] F. Özel and P. Freire, Ann. Rev. Astron. Astrophys. **54**, 401 (2016); arXiv:1603.02698 [astro-ph.HE].
[72] J. Antoniadis et al., Science **340**, 1233232 (2013).
[73] F. J. Fattoyev, J. Piekarewicz, and C. J. Horowitz, Phys. Rev. Lett. **120**, 172702 (2018).
[74] J. M. Lattimer and M. Prakash, Phys. Rept. **442**, 109 (2007).
[75] A. G. Lyne et al., Science **303**, 1153 (2004), astro-ph/0401086.
[76] M. Kramer and N. Wex, Class. Quantum Grav. **26**, 073001 (2009).
[77] J. M. Lattimer and B. F. Schutz, Astrophys. J. **629**, 979 (2005), astro-ph/0411470.
[78] Philippe Landry and Bharat Kumar, arXiv:1807.04727v2 [gr-qc].